RSC Advances

PAPER

View Article Online
View Journal | View Issue



Cite this: *RSC Adv.*, 2024, **14**, 34661

# Highly sensitive detection of alpha-fetoprotein using sandwich sensors†

Bing Xie,[a] Huixing Wang,[b] Zaina Omary Mochiwa,[b] Dingjie Zhou*[c] and Li Gao *[b]

Alpha-fetoprotein (AFP) is a crucial biomarker for detecting certain tumors across various demographics, including men, non-pregnant women, and children. However, existing detection methods often lack the desired sensitivity, necessitating the development of a straightforward, dependable, and highly sensitive AFP detection method. In this study, a novel approach utilizing a sandwich sensor system designed around the GDYO@AuNPs@PCN (graphdiyne oxide, gold nanoparticle, and porous coordination network) composite was proposed. The results revealed that this composite material, comprising three key components, offers superior quenching capabilities and heightened sensitivity to AFP compared to DNA sensors employing different nanomaterials. Leveraging the distinctive advantages and properties of the composite material, a "three in one" structure was devised by integrating two aptamers with AFP to form an efficient "sandwich" configuration for AFP capture. Additionally, the inclusion of antifouling peptides in the system effectively mitigates non-specific adsorption of AFP on the sensing interface, ensuring a high signal-to-noise ratio. Notably, the sandwich sensor employing the "three in one" composite with peptides achieves a limit of detection (LOD) of 1.51 pg mL$^{-1}$, indicative of its ability to reduce background signals, facilitate efficient AFP binding, and enhance sensitivity. Furthermore, the sensor exhibited promising performance and demonstrated consistent results in serum samples, emphasizing its promising practical applications.

Received 15th August 2024
Accepted 22nd October 2024

DOI: 10.1039/d4ra05930a

rsc.li/rsc-advances



## 1. Introduction

Alpha-fetoprotein (AFP), the most commonly used protein biomarker, has attracted significant attention in recent years.[1] AFP is of great significance in detecting certain tumors in men, non-pregnant women, and children as a biomarker. Compared to normal levels, elevated levels of AFP in the bloodstream of adults could signal the presence of specific cancer types, notably hepatocellular carcinoma (HCC), gastric cancer, pancreatic cancer, ovarian cancer, or testicular cancer. According to statistics, AFP levels significantly increase to 500 ng mL$^{-1}$ in nearly 75% of HCC patients.[2] Additionally, AFP detection indicators are particularly important for identifying early curable tumors in high-risk yet asymptomatic populations, thereby reducing disease-related mortality and improving cost-effectiveness. The advancement of AFP detection technology is requisite for the early detection of certain cancers and the clinical detection of AFP.

To facilitate early tumor detection and clinical assessment through alpha-fetoprotein (AFP) detection, the advancement of highly sensitive AFP detection technologies is imperative. Various methods have been previously devised for AFP detection, including enzyme-linked immunosorbent assay (ELISA), radioimmunoassay, fluorescence immunoassay, electrochemiluminescence, Raman spectroscopy, and electrochemical immunosensing, among others.[3–7] However, these methods are limited by issues such as non-specific binding and are not suitable for high-throughput analysis.[8] Additionally, these methods face challenges like high cost, the need for trained technicians, extended analysis times, and limited dynamic range. Consequently, there's a critical need for developing AFP detection methods that are rapid, highly sensitive, selective, cost-effective, and efficient, to improve human disease diagnosis.

Utilizing nanomaterials like gold nanoparticles and graphdiyne oxides can significantly enhance the compatibility and detection sensitivity of biomarkers. For instance, Nargish Parvin *et al.*[9] in 2017, demonstrated through density functional theory (DFT) calculations that GDYO had a better quenching effect compared to GO. This enhanced quenching effect of GDYO contributes to the increased detection sensitivity by improving the signal-to-noise ratio, making it a superior material for fluorescence-based sensing applications. Moreover, multifunctional porous materials have emerged as key components in sensor development.[10,11] Metal–organic frameworks, composed of metal ions and organic ligands, represent one such category.[12] These materials possess adjustable pore size and a large surface area, offering catalytic, magnetic, and separation properties.[13]

[a]*The Fourth Affiliated Hospital of Jiangsu University, Zhenjiang 212001, China*
[b]*School of Life Sciences, Jiangsu University, Zhenjiang 212013, China. E-mail: gaoli@ujs.edu.cn*
[c]*Jiangsu Health Development Research Center, NHC Contraceptive Aduerse Reaction Surveillance Center, Jiangsu Provincial Medical Key Laboratory of Fertility Protection and Health Technology Assessment, Nanjing 210036, China*

† Electronic supplementary information (ESI) available. See DOI: https://doi.org/10.1039/d4ra05930a

Consequently, they can be applied to gas adsorption,[14] luminescence,[15] sensing technology,[16] and heat conversion.[17] Notably, the porous coordination network (PCN) within porphyrin-based metal–organic frameworks has attracted increasing attention due to its high loading efficiency and its ability to avoid self-quenching of photosensitizers.[18] MOFs represent porous inorganic–organic hybrid materials featuring periodic network structures formed by self-assembling metal ions and organic ligands. Due to their structural diversity, flexibility, variability, and unique chemical and porous structures, MOFs possess inherent fluorescence quenching characteristics, rendering them ideal materials for use in fluorescent biosensors.[19] Sandwich-type biosensors usually consist of a recognition unit such as a capture anti-body (Ab1) immobilized on the surface, and a signal probe (for example, enzyme or redox label) conjugated with the detection antibody (Ab2). Signal amplification serves as a common strategy to enhance the detection sensitivity of sandwich-type biosensors.

Aggregation-induced emission (AIE) is depicted as a unique photophysical phenomenon that stands in contrast to aggregation-induced quenching. AIE fluorophore emits because of aggregation. In this study, DSAI with the AIE effect was employed to construct a label-free fluorescent biosensor. This biosensor capitalizes on the quenching effect of AuNPs and aptamers for the detection of AFP. Additionally, a porous coordination network (PCN), a subset of metal–organic frameworks (MOFs), was utilized. The structure of GDYO was used to form a complex with AuNPs, aiming to enhance the sensitivity of AFP detection. Subsequently, PCN and (polyethylene glycol) PEG were introduced into the GDYO@AuNPs system, resulting in the formation of a complex (GDYO@AuNPs@PCN). The sensitivity of AFP detection was then compared between these configurations. As a control, the aptamer chain without AIE functionality interacted with the GDYO@AuNPs@PCN after covalent immobilization which depicts that a specific sequence of nucleic acids (aptamer) lacking Aggregation-Induced Emission (AIE) properties was able to engage with a complex nanomaterial composed of GDYO, AuNPs, and PCN after being permanently attached to it through stable covalent bonds.

Meanwhile, the aptamer chain with AIE functionality was introduced to form a sensing platform similar to the "sandwich" structure. The multifunctional antifouling peptide was added to reduce the background signal, facilitating the efficient interaction between the aptamer and AFP.

# 2. Materials and methods

## 2.1 Chemical reagents and experimental materials

| | |
|---|---|
| Aptamer | 5′-GTG ACG CTC CTA ACG CTG ACT CAG GTG CAG TTC TCG ACT CGG TCT TGA TGT GGG TCC TGT CCG TCC GAA CCA ATC-SH-3′ |
| Aptamer-1 | 5′-GTG ACG CTC CTA ACG CTG ACT CAG GTG CAG TTC TCG ACT CGG TCT TGA TGT GGG TCC TGT CCG TCC GAA CCA ATC-3′ |
| Peptide | EKEKEKEPPPC |

The aptamer[20] and the peptide EKEKEKEPPPC,[4] were purchased from Sangon Biotech. (Shanghai, China) Co., Ltd. Chloroauric acid ($HAuCl_4$) was purchased from Sigma-Aldrich, while sodium citrate ($C_6H_5Na_3O_7$) was sourced from Sinopharm Chemical Reagent Co., Ltd. DSAI (4,4′-(1*E*,1′*E*)-2,2′-(anthracene-9,10-diyl) bis(ethene-2,1-diyl)bis(*N*,*N*,*N*-trimethylbenzenaminium) iodide) powder (Cat#QY-C-12272) and PCN (the molecular formula is $C_{96}H_{68}N_8O_{32}Zr_6$, size is 200 × 20 nm) were acquired from Xi'an Qiyue (Xi'an, China) Biotechnology Co., Ltd.[21] GDYO powder (50–80 nm) was synthesized from graphdiyne powder by a modified Hummer's method[22] and obtained from Xianfeng (Nanjing, China) Nanomaterial Technology Co., Ltd. The beef serum was obtained from Tianhang Biotechnology Co., Ltd. (Huzhou, China).

## 2.2 Experimental instruments

All fluorescence spectra and required absorbance readings were collected and recorded using a Bio-Tek Synergy $H_4$ multifunctional microplate reader, with an excitation wavelength of 428 nm. The emission wavelength range was set at 550 nm. A constant temperature magnetic stirrer was used to heat and stir the samples. Gold nano-particles were prepared using a DF-101S magnetic stirrer.

## 2.3 Preparation of AuNP nanoparticles

The gold nanoparticles were prepared using the classical Frens method,[23] specifically the trisodium citrate reduction technique. First, a 0.01% aqueous solution of chloroauric acid was heated with continuous stirring until it reached boiling. Then, a 1% aqueous solution of trisodium citrate was added, and the mixture was boiled for 15 minutes. Afterward, it was stirred while cooling to room temperature.

## 2.4 Preparation of GDYO@AuNPs@PCN composite

Following the method reported by Huang *et al.*,[24] the GDYO@AuNPs@PCN composite was prepared. This involved creating a 1 mL solution with a concentration of (2 mg $mL^{-1}$) of the GDYO@AuNPs complex using ultrasonic techniques to ensure uniformity. Next, 400 μL of a PCN solution at a concentration of (0.1 mg $mL^{-1}$) was slowly added to the GDYO@AuNPs complex solution. This addition was facilitated by the presence of hydrazine hydrate (10 μL $NH_2NH_2 \cdot H_2O$, 90% analytical reagent).

## 2.5 Detection of alpha-fetoprotein by complex and antifouling peptide based on GDYO@AuNPs@PCN

To detect alpha-fetoprotein (AFP) using the GDYO@AuNPs@PCN composite, a uniformly dispersed solution of GDYO@AuNPs was synthesized at a concentration of 15 μg $mL^{-1}$. The solution was centrifuged to remove any aggregates, adjusted to a constant volume, and thoroughly mixed. Subsequently, PCN was incorporated into the GDYO@AuNPs and resulted in the final GDYO@AuNPs@PCN composite. The fluorescence intensity of this composite solution was measured at 550 nm. Following this, AFP was added to the solution, and

the fluorescence intensity was measured again at the same wavelength. The change in fluorescence intensity, expressed as $(F/F_0 - 1)$, where $F$ and $F_0$ represent the fluorescence intensity of the sensing system at 550 nm before and after adding AFP, respectively, was calculated.

The aptamer with a 3′ terminal thiol group was mixed with GDYO@AuNPs@PCN in the total system, with the complex comprising 500 μL. Aptamer can be connected on the surface of Au NPs using the Au–S reaction. After incubating in a 10 mM PBS buffer (pH 7.4) for 12 h, the sample was centrifuged at 13 000 rpm for 30 min. The supernatant was then collected to measure the initial fluorescence intensity, denoted as $F_0$. Next, a final concentration of 300 ng mL$^{-1}$ peptide and varying concentrations of AFP were added, allowing the reaction to proceed for 30 min at room temperature. The final concentration of aptamer-1 with DSAI (10 μM) was added, and the reaction time was continued for 30 min. After centrifugation, 200 μL of the supernatant was measured for its fluorescence intensity, denoted as $F$. Here, $F_0$ and $F$ respectively represent the fluorescence intensity of the fluorescence sensing system before and after adding AFP at 550 nm.

At the end of the peptide EKEKEKEPPPC, C has an SH group that can be connected on the surface of AuNP using Au–S reaction. So, the antifouling peptide-functionalized with the GDYO@AuNPs@PCN composite was used to enhance the specificity and selectivity of the detection. The composite was treated with an antifouling peptide to prevent nonspecific binding of other proteins. For selectivity analysis, AFP and other protein analogues were introduced at a concentration of 0.5 ng mL$^{-1}$. The fluorescence response to these analogues was measured to demonstrate the selectivity of the GDYO@AuNPs@PCN composite for AFP.

# 3. Results and discussion

## 3.1 Detection principle and method of sensor based on sandwich

In the presence of aptamer, DSAI molecules aggregate on aptamer through the intercalation and the electrostatic interaction as well as the hydrophobic interaction, resulting in the strong fluorescence in the solution.[25] In previous studies, DNA sensors utilizing various nanomaterials, including a three-material composite nano quencher, have demonstrated significant quenching effects for FAM-labeled DNA (6-carboxyfluorescein).[26] While these studies focused on DNA sensing applications, our current work extends this approach to the detection of alpha-fetoprotein (AFP). Based on the promising results from these DNA sensors, we hypothesized that the GDYO@AuNPs@PCN composite would also exhibit a strong quenching effect and high sensitivity for AFP detection. Therefore, we investigated the performance of our composite material in quenching fluorescence and detecting AFP. Leveraging these advantages and characteristics of the composite materials, two aptamers and AFP were combined to form a more efficient "sandwich" structure for AFP detection. To maintain a high signal-to-noise ratio, the sensor should selectively bind to the target while minimizing biofouling,

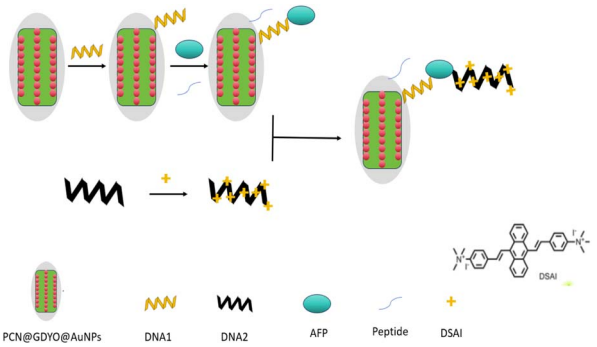


Fig. 1 Sandwich structure based on PCN@GDYO@AuNPs complex and antifouling peptide. The aptamer with a 3′ terminal thiol group was mixed with GDYO@AuNPs@PCN. After centrifugation, a final concentration of 300 ng mL$^{-1}$ peptide and varying concentrations of AFP were added. The final concentration of aptamer-1 with DSAI (10 μM) was added.

which mainly affects sensors through non-specific interactions.[27] To address this issue, antifouling peptides were introduced into the system to resist the non-specific adsorption of AFP on the sensing interface as shown in Fig. 1.

## 3.2 Optimization of experimental conditions based on sandwich structure

To optimize the experimental conditions and achieve the best detection results for AFP on the composite-based sandwich structure sensing platform, various parameters were fine-tuned. This optimization process included adjusting the concentrations of the complex aptamer, peptide, and other relevant factors.

## 3.3 Optimization of GDYO@AuNPs@PCN complex concentration

The optimal concentration of composite nanomaterials was determined by adding different concentrations (5, 10, 15, 20, and 25 μg mL$^{-1}$), 30 nM aptamer, and 10 nM aptamer-1 with DSAI (10 μM) to the sensing system without peptide. AFP was introduced at a concentration of 0.5 ng mL$^{-1}$. TEM of GDYO@AuNPs@PCN composite was shown in Fig. S9.† The fluorescence intensity was measured before and after adding AFP, allowing the comparison of the fluorescence change rate at each concentration. The results, depicted in Fig. 2, showed that as the concentration of the composite increased, the fluorescence change rate also increased, peaking at 15 μg mL$^{-1}$. Beyond this point, the fluorescence change rate gradually decreased. A lower concentration might not allow sufficient immobilization of the aptamer, while a higher concentration improves the cost. Therefore, 15 μg mL$^{-1}$ GDYO@AuNPs@PCN was selected as the optimal concentration.

## 3.4 Optimization of aptamer concentration

Aptamers (thiol-labeled aptamers) at concentrations of 5 nM, 10 nM, 20 nM, 30 nM, and 40 nM, and 10 nM aptamer-1 with DSAI (10 μM) were added to the sensor including 15 μg mL$^{-1}$

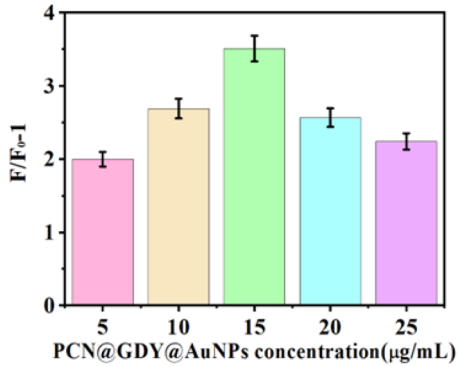


Fig. 2 Effect of different concentrations of GDYO@AuNPs@PCN composites on the fluorescence intensity.

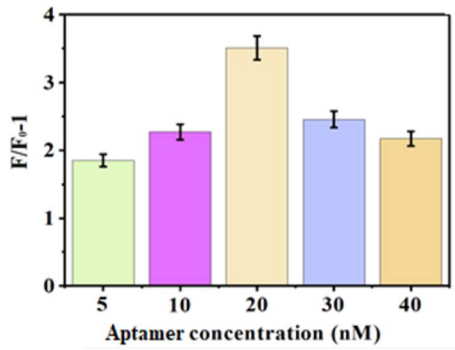


Fig. 3 Effect of different concentrations of aptamer on fluorescence intensity.

GDYO@AuNPs@PCN composite and without peptide. AFP was introduced at a concentration of 0.5 ng $mL^{-1}$. The changes in fluorescence intensity are shown in Fig. 3. Notably, the fluorescence intensity change was highest when the aptamer concentration was 20 nM, compared to other concentrations. When the concentration of aptamer reached 20 nM, the fluorescence intensity reached its limit. However, an increase in the concentration of aptamer can improve the background value and result in a decrease in the $F/F_0 - 1$ value. Excess aptamer can interfere with the reaction between aptamer with AIE and AFP. So these resulted in the decrease in fluorescence intensity with the increase of aptamer concentration. Consequently, 20 nM was selected as the optimal concentration for the sensor.

### 3.5 Optimization of antifouling peptide concentration

To determine the optimal effect of the peptide on the reaction system, various concentrations of peptide (0, 100, 200, 300, 400, and 500 ng $mL^{-1}$) were tested with 20 nM aptamer, 15 μg $mL^{-1}$ GDYO@AuNPs@PCN, 10 μM DSAI and 0.5 ng $mL^{-1}$ AFP. The analysis of the change in $F/F_0 - 1$ before and after the addition of AFP, as shown in Fig. 4, demonstrated a significant improvement in the sensing system when peptides were added, compared to when they were not. Peptides resist the non-specific adsorption of AFP on the sensing interface. At

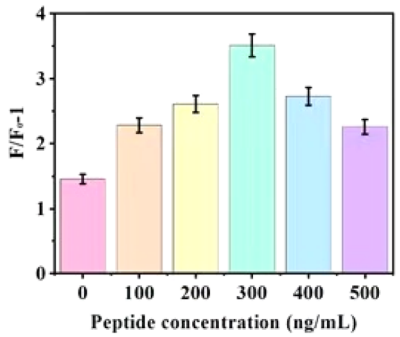


Fig. 4 Effect of different concentrations of peptides on fluorescence intensity.

a peptide concentration of 300 ng $mL^{-1}$, the reaction system exhibited the best overall performance, making this the optimal condition for the experiment. In Fig. 4b, the fluorescence response ($F/F_0 - 1$) values are specific to the detection of AFP using the GDYO@AuNPs@PCN sensor, while Fig. 5 depicts the response for a peptide under different experimental conditions.

### 3.6 Sensitivity analysis of GDYO@AuNPs@PCN compound

Based on the optimized experimental conditions, various concentrations of AFP (0.01, 0.05, 0.1, 0.5, 0.8, 1, 5, and 8 ng $mL^{-1}$) were added to the complex including 20 nM aptamers and 15 μg $mL^{-1}$ GDYO@AuNPs@PCN in a PBS buffer. 10 nM

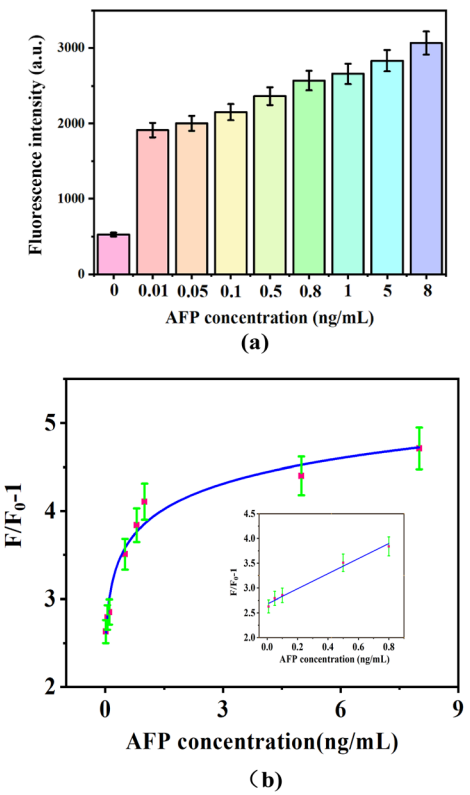


Fig. 5 Different AFP concentrations induced fluorescence intensity (a) and (b) fluorescence changed at a 300 ng $mL^{-1}$ peptide concentration.

Table 1 Comparison of the AFP detection methods

| Detection method | Materials | Linear range | LOD | References |
|---|---|---|---|---|
| SERS | AFP aptamer/IgG | 50–100 ng $mL^{-1}$ | 50 pg $mL^{-1}$ | 28 |
| FRET | AFP aptamer/magnetic gold nanocomposites | 0.005–0.1 ng $mL^{-1}$ | 1.429 pg $mL^{-1}$ | 3 |
| FRET | AFP aptamer/QDs-AuNPs | 0.5–45 ng $mL^{-1}$ | 400 pg $mL^{-1}$ | 29 |
| FRET | FAM-labeled AFP aptamer/PdNP | 5–150 ng $mL^{-1}$ | 1.38 ng $mL^{-1}$ | 30 |
| DPV | Thionin/reduced graphene oxide/gold nanoparticles/ aptamer | 0.1–00.0 μg $mL^{-1}$ | 0.05 μg $mL^{-1}$ | 31 |
| EIS | Epitope molecularly imprinted polymer film | $1.0 \times 10^{-4}$ – 1000 ng $mL^{-1}$ | 0.075 pg $mL^{-1}$ | 32 |
| FRET | GDYO@AuNPs@PCN complex/aptamer | 0.01–0.8 ng $mL^{-1}$ | 1.51 pg $mL^{-1}$ | This work |

aptamer-1 and 300 ng $mL^{-1}$ peptide were added and incubated at room temperature for 30 minutes. The fluorescence value was recorded at 550 nm, and the corresponding change in fluorescence intensity from aptamer with DSAI was calculated. The results, depicted in Fig. 5a, show that the fluorescence value increases with higher AFP concentrations. Fig. 5b illustrates a clear linear relationship between $F/F_0 - 1$ and AFP concentrations in the range of 0.01–0.8 ng $mL^{-1}$. The linear regression equation was determined to be $F/F_0 - 1 = 1.501 \times C[\text{AFP}] + 2.686$, $R^2 = 0.98$. The detection limit was calculated to be 1.51 pg $mL^{-1}$. As shown in Table 1, this sensor exhibits a lower limit of detection and a wider linear range compared to most reported sensors, demonstrating superior performance.

### 3.7 Selectivity analysis based on sandwich structure

To assess the sensor's selectivity, we examined various substances with similarities to AFP, including BSA, CEA, HSA, IgG, and thrombin, under identical experimental conditions. Both AFP and these analogues were introduced at a concentration of 0.5 ng $mL^{-1}$, following the established optimal conditions. Subsequently, we measured the fluorescence intensity and the change ($F/F_0 - 1$) before and after the addition of the respective proteins. The findings, displayed in Fig. 6, demonstrate AFP is distinguished from other interfering substances at low concentrations, indicating the sensor's favorable selectivity towards AFP.

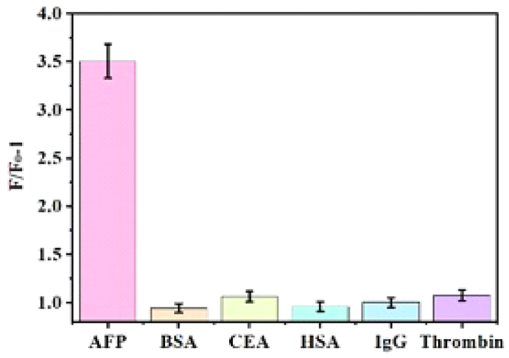


Fig. 6 Under optimal conditions, AFP was selected with other analogues such as BSA, CEA, HSA, IgG, and thrombin. Both AFP and these analogues were introduced at a concentration of 0.5 ng $mL^{-1}$.

### 3.8 Analysis of serum samples

Two serum samples were detected using this sensor. Sample 1 was the serums of patients with hepatic malignant tumor. Sample 2 was the serum of a normal person. The hepatopathy serum (Sample 1) was diluted 800 folds and the serum of normal person (Sample 2) was diluted 400 folds before detection because of the higher concentration of AFP in the serum of hepatopathy patients. The results were shown in Table 2. The concentrations of AFP in the hepatopathy serum were higher than that of normal person. The determined concentrations for AFP using this method were similar to that obtained using electrochemiluminescence immunoassay (ECLIA) in the hospital.

To assess the stability of the sensor in clinical settings, the original reaction system was replaced with a sensor in the serum. Three different concentrations of AFP (0.05 ng $mL^{-1}$, 0.1 ng $mL^{-1}$, and 0.5 ng $mL^{-1}$, diluted in PBS buffer) within the linear range were selected for standard recovery tests in beef serum. Each group was tested three times. As shown in Table 3, the recovery rates for the three groups of samples were 108%, 102%, and 99.6%, respectively. The relative standard deviation, calculated to be between 3.42% and 4.11%, met the relevant practical application requirements. These results indicate that the method is reliable and provides a theoretical basis for the clinical application of AFP with practical significance.

Table 2 Detection of AFP concentrations in the serum samples

| Methods | Sample 1 (ng $mL^{-1}$) | Sample 2 (ng $mL^{-1}$) |
|---|---|---|
| This method ($n = 3$) | 198.34 ± 11.23 | 3.89 ± 1.04 |
| Electrochemiluminescence immunoassay (ECLIA) ($n = 1$) | 195.45 | 3.84 |

Table 3 Results of spiking/recovery experiments for AFP detection

| Samples | Added (ng $mL^{-1}$) | Obtained (ng $mL^{-1}$) | Recovery (%) | RSD (%) |
|---|---|---|---|---|
| 1 | 0.05 | 0.054 | 108 | 3.42 |
| 2 | 0.1 | 0.102 | 102 | 4.11 |
| 3 | 0.5 | 0.498 | 99.6% | 3.78 |

## 4. Conclusions

In this study, it was observed that GDYO@AuNPs exhibited a higher sensitivity to AFP compared to AuNPs alone (Fig. S6 and S12†). Furthermore, the detection sensitivity of GDYO@AuNPs@PCN was found to be significantly improved, leading to a lower detection limit of 3.39 μg $mL^{-1}$ AFP (Fig. S13†) compared to 4.81 μg $mL^{-1}$ AFP with AuNPs alone (Fig. S6†). This indicates a superior quenching effect for the tricomponent nanocomposite compared to the individual materials under the same conditions. Additionally, the composite demonstrated enhanced fluorescence quenching capabilities, achieving higher sensitivity than each single material. A sandwich sensor system designed based on the GDYO@AuNPs@PCN complex, including two aptamers alongside the 3-in-1 composite material, showed a detection limit of 1.51 pg $mL^{-1}$, effectively minimizing background signals, facilitating more efficient interaction with AFP, and ultimately improving overall sensitivity. While the GDYO@AuNPs@PCN-based detection system exhibits promising sensitivity and a low detection limit, limitations include the complex and time-consuming synthesis of the tricomponent nanocomposite, which may affect reproducibility and scalability, and the need for further investigation into its stability over time and under various conditions. Future perspectives involve optimizing the synthesis process for better reproducibility, exploring cost-effective alternative materials, integrating the sensor into portable devices for point-of-care testing, and conducting additional studies to validate its specificity in complex biological samples.

## Data availability

All relevant data are within the paper.

## Conflicts of interest

There are no conflicts to declare.

## Acknowledgements

This work was supported of Medical Research Project of the Jiangsu Provincial Health Commission (M2021092), the Independent Research Project of Jiangsu Provincial Health Development Research Center (JSHD2021061), the Jiangsu Maternal and Child Health Research Project (F202144), Guiding Science and Technology Plan Project for Social Development in Zhenjiang City (FZ2022052), Zhenjiang Science and Technology Plan (Social development, SH2024030 and SH2024098), Jiangsu University Medical Education Collaborative Innovation Fund (JDYY2023082), Open Project of Clinical Medical Research Center for Obstetrics and Gynecology in Zhenjiang City (SS2022003-KFB02), and National Natural Science Foundation of China (NSAF, No. U2230132).

## References

1 J. Li, T. Gao, S. Gu, J. Zhi, J. Yang and G. Li, *Biosens. Bioelectron.*, 2017, **87**, 352–357.
2 L. Liu, H. Wang, B. Xie, B. Zhang, Y. Lin and L. Gao, *Biosens*, 2022, **12**, 780.
3 L. Liu, H. Wang, H. Sulemana, B. Xie and L. Gao, *Biosens*, 2023, **13**(3), 351.
4 Y. Wang, M. Cui, M. X. Jiao and X. L. Luo, *Anal. Bioanal. Chem.*, 2018, **410**, 5871–5878.
5 Z. Chen, H. Wang, Z. Zhang and L. Chen, *Anal. Chem.*, 2019, **91**, 1254–1259.
6 Y. Li, L. Dong, X. Wang, Y. Liu, H. Liu and M. Xie, *Spectrochim. Acta, Part A*, 2018, **196**, 103–109.
7 A. Verdin, C. Malherbe and G. Eppe, *Microchim. Acta*, 2021, **188**, 228.
8 C. Wang, P. Yu, S. Guo, L. Mao, H. Liu and Y. Li, *Chem. Commun.*, 2016, **52**(32), 5629–5632.
9 N. Parvin, Q. Jin, Y. Wei, R. Yu, B. Zheng, L. Huang, Y. Zhang, L. Wang, H. Zhang, M. Gao, H. Zhao, W. Hu, Y. Li and D. Wang, *Adv. Mater.*, 2017, **29**, 1606755.
10 Y. Yan, Z. Liu, W. Pang, S. Huang, M. Deng, J. Yao, Q. Huang, M. Jin and L. Shui, *Biosens. Bioelectron.*, 2024, **262**, 116528.
11 Z. Liu, Q. Huang, J. Chen, J. Yao, M. Jin, X. Wang, E. Akinoglu, M. Zhang, N. Li and L. Shui, *J. Electroanal. Chem.*, 2021, **883**, 115068.
12 Z. Liu, S. Huang, Y. Yan, W. Pang, F. Zhong, Q. Huang, F. Caddeo, M. Zhang, M. Jin and L. Shui, *Talanta*, 2024, **272**, 125735.
13 S. Huang, Z. Liu, Y. Yan, J. Chen, R. Yang, Q. Huang, M. Jin and L. Shui, *Biosens. Bioelectron.*, 2022, **207**, 114129.
14 S. Shi, K. Li, Y. Li, Z. Ma, S. Qi, X. Liu and L. Sun, *ACS Mater. Lett.*, 2023, **5**(8), 2189–2196.
15 S. Zhang, J. Huang, L. Wang, H. Li, H. Dong, Q. Zhu, Y. Wen and X. Wu, *Adv. Opt. Mater.*, 2024, **12**(19), 2400213.
16 H. Jeong, G. Park, J. Jeon and S. Park, *Acc. Chem. Res.*, 2024, **57**(16), 2336–2346.
17 X. Chang, T. Yan, W. Pan and L. Wang, *Appl. Therm. Eng.*, 2024, **255**, 124046.
18 S. Wan, J. Zeng, H. Cheng and X. Zhang, *Biomaterials*, 2018, **185**, 51–62.
19 L. Gao, Y. Deng, H. Liu, K. Solomon, B. Zhang and H. Cai, *Biosen*, 2022, **12**, 745.
20 G. Li, J. Zeng, H. Liu, P. Ding, J. Liang, X. Nie and Z. Zhou, *Mikrochim. Acta*, 2019, **186**(5), 314.
21 X. Li, K. Ma, S. J. Zhu, S. Y. Yao, Z. Y. Liu, B. Xu, B. Yang and W. J. Tian, *Anal. Chem.*, 2014, **86**, 298–303.
22 W. S. Hummers Jr and R. E. Offeman, *J. Am. Chem. Soc.*, 1958, **80**, 1339.
23 G. Frens, *Nat. Phys. Sci.*, 1973, **241**, 20–22.
24 X. Huang, Z. He, D. Guo, Y. Liu, J. Song, B. C. Yung, L. Lin, G. Yu, J. Zhu, Y. Xiong and X. Chen, *Theranostics*, 2018, **8**(13), 3461–3473.
25 K. Ma, H. Wang, H. Li, B. Xu and W. Tian, *Sens. Actuators, B*, 2017, **253**, 92–96.

26 I. Khalil, W. A. Yehye, N. M. Julkapli, S. Rahmati, A. A. I Sina, W. J. Basirun and M. R. Johan, *Biosens. Bioelectron.*, 2019, **131**, 214–223.
27 Y. Zhang, N. Islam, R. G. Carbonell and O. J. Rojas, *Anal. Chem.*, 2013, **85**(2), 1106–1113.
28 Q. Wang, Y. Hu, N. Jiang, J. Wang, M. Yu and X. Zhuang, *Bioconjugate Chem.*, 2020, **31**, 813–820.
29 L. Zhou, F. Ji, T. Zhang, F. Wang, Y. Li, Z. Yu, X. Jin and B. Ruan, *Talanta*, 2019, **197**, 444–450.
30 G. Li, J. Zeng, H. Liu, P. Ding, J. Liang, X. Nie and Z. Zhou, *Mikrochim. Acta*, 2019, **186**, 314.
31 G. Li, S. Li, Z. Wang, Y. Xue, C. Dong, J. Zeng, Y. Huang, J. Liang and Z. Zhou, *Anal. Biochem.*, 2018, **547**, 37–44.
32 H. Shao and Z. Liu, *Electrochim. Acta*, 2024, **484**, 144094.